This is a preprint, the final version is subject to change, of the American Mineralogist (MSA)
Cite as Authors (Year) Title. American Mineralogist, in press.
DOI: https://doi.org/10.2138/am-2018-6499

1 **Rivision 1**

2 Stability of Al-bearing superhydrous phase B at the mantle transition zone and the
3 uppermost lower mantle

4 Sho Kakizawa[1*], Toru Inoue[1,2,3], Hideto Nakano[1], Minami Kuroda[4], Naoya Sakamoto[5], and
5 Hisayoshi Yurimoto[4,5,6]

6 [1]Geodymanics Research Center, Ehime University, Matsuyama, Ehime 790-5877, Japan

7 [2]Department of Earth and Planetary Systems Science, Hiroshima University,
8 Higashi-Hiroshima, Hiroshima 739-8526, Japan

9 [3]Hiroshima Institute of Plate Convergence Region Research (HiPeR), Hiroshima University,
10 Higashi-Hiroshima, Hiroshima 739-8526, Japan

11 [4]Department of Natural History Sciences, Hokkaido University, Sapporo, Hokkaido
12 060-0810, Japan

13 [5]Isotope Imaging Laboratory, Hokkaido University, Sapporo, Hokkaido 001-0021, Japan

14 [6]Institute of Space and Astronautical Science, JAXA, Sagamihara, Kanagawa 252-5120,
15 Japan

16 ***Corresponding author**

17 E-mail address: kakizawa@sci.ehime-u.ac.jp

18

This is a preprint, the final version is subject to change, of the American Mineralogist (MSA)
Cite as Authors (Year) Title. American Mineralogist, in press.
DOI: https://doi.org/10.2138/am-2018-6499

Abstract

We determined the stability and chemical composition of Al-bearing superhydrous phase B at 20-24 GPa and 1400-2000°C to discuss the mechanism of water transport in the mantle transition zone and uppermost lower mantle at temperatures close to the mantle geotherm. Superhydrous phase B contained significant amounts of Al_2O_3, from 14 to 32 wt%, and Al-bearing superhydrous phase B remained stable, even at 2**0**0°C and pressures of approximately 20-24 GPa. Moreover, two types of superhydrous phase B with different chemical compositions coexisted at 20-24 GPa and 1600°C. The Al_2O_3 and H_2O contents increased, and the MgO and SiO_2 contents decreased as the pressure and temperature increased up to 1600°C. Above 1600°C, the MgO and Al_2O_3 contents increased, and the SiO_2 and H_2O contents decreased as the temperature increased. We found two substitution mechanisms: (i) $2Mg^{2+} + Si^{4+} \rightleftarrows 2Al^{3+} + 2H^{+} + V_{Mg}$ (Mg site vacancy) ($2Mg^{2+} = Al^{3+} + H^{+} + V_{Mg}$) : ($Si^{4+} = Al^{3+} + H^{+}$) = 1:1, (ii) $Si^{4+} + 16H^{+} \leftrightarrows 4Mg^{2+} + 4Al^{3+}$. The maximum H_2O content of Al-bearing superhydrous phase B is 11.1(3) wt%, which is ~1.9 times larger than that of the Mg-endmember. The crystal structures of the two coexisting superhydrous phase Bs are expected to be slightly different from each other. The present results indicate that Al-bearing superhydrous phase B can be stable in a subducted slab with a high Al content

compared to pyrolite (e.g, chlorite) at temperatures typical of the mantle transition zone and

the lower mantle. Thus, water can be transported to the lower mantle by Al-bearing superhydrous phase B in the subducting slab, even at the typical mantle geotherm.

This is a preprint, the final version is subject to change, of the American Mineralogist (MSA)
Cite as Authors (Year) Title. American Mineralogist, in press.
DOI: https://doi.org/10.2138/am-2018-6499

Introduction

Water strongly affects several key properties of the deep mantle, such as melting temperature, rheological properties, and electrical conductivity, etc. (e.g., Inoue, 1994, Karato et al., 1986; Yoshino et al., 2006). Water is transported into the Earth's deep interior by hydrous minerals in cold subducted slabs. Recently, hydrous ringwoodite containing ~1.5 wt% water was discovered as an inclusion in an ultra-deep diamond (Pearson et al., 2014). This observation implies that, at least locally, the mantle transition zone contains water. The stability of hydrous phases has been studied in peridotite, basalt, and sediment (e.g., Litasov and Ohtani., 2003; Schmidt and Poli, 1998; Ono, 1998). The important hydrous phases in hydrous peridotite with increasing pressure include serpentine ($Mg_3Si_2O_5(OH)_4$), phase A ($Mg_7Si_2O_8(OH)_6$), phase E ($Mg_{2.3}Si_{1.3}H_{2.4}O_6$), superhydrous phase B ($Mg_{10}Si_3O_{14}(OH)_4$), phase D ($MgSi_2O_4(OH)_2$), and phase H ($MgSiO_2(OH)_2$). These phases are called dense hydrous magnesium silicates (DHMSs).

Superhydrous phase B has a composition of $Mg_{10}Si_3O_{14}(OH)_4$ and contains 5.8 wt% H_2O. The stability of superhydrous phase B was studied in the MgO-SiO_2-H_2O system (Gasparik, 1993; Irifune et al., 1998; Ohtani et al., 2001, 2003, 2004; Litasov and Ohtani, 2003). Gasparik (1993) observed superhydrous phase B coexisting with stishovite at 16-24 GPa and 800-1400°C. In hydrous peridotite, superhydrous phase B is stable with phase D

above 20 GPa and up to 1100°C (Kawamoto, 2004; Litasov et al., 2008). Ohtani et al. (2003) determined the decomposition boundary of superhydrous phase B and located it at approximately 28 GPa and 1200°C. The stability field of superhydrous phase B suggests that it is an important phase in the mantle transition zone and the uppermost lower mantle at the same temperature as a subducted slab. All Mg-Si endmembers of DHMSs, including superhydrous phase B, breakdown at temperatures below the typical mantle geotherm.

Recent studies suggest that incorporation of Al increases the high-temperature stability of these hydrous minerals. Al-bearing phase D breaks down at ~1600°C and 24 GPa, which is approximately 200°C higher than that of Mg-endmember phase D (Ghosh and Schmidt, 2014). Moreover, Al-endmember phase D (Al-phase D, $Al_2SiO_4(OH)_2$) is stable at a temperature of over 2000°C and pressure of 26 GPa (Pamato et al., 2015). In the case of phase H, it can form a solid solution with δ-AlOOH (Nishi et al., 2014) and this solid solution is stable even along a typical mantle geotherm (Ohira et al., 2014). On the other hand, phase A cannot contain Al. Instead, Al is included in 23 Å phase ($Mg_{11}Al_2Si_4O_{16}(OH)_{12}$), which has stability region similar to phase A (Cai et al., 2015). However, the effect of Al on the stability of superhydrous phase B is not known.

To clarify the stability of Al-bearing superhydrous phase B in the mantle transition zone and the uppermost lower mantle under a typical mantle geotherm, we conducted

high-pressure and high-temperature experiments using a multi-anvil apparatus. Recovered samples were analyzed with a scanning electron microscope with energy-dispersive X-ray spectrometer (SEM-EDS) and a secondary ion mass spectrometer (SIMS). Here, we report the stability and chemical composition of Al-bearing superhydrous phase B, and we will also discuss a mechanism of water transport to the lower mantle.

Experimental and analytical methods

The starting materials for these experiments were powdered mixtures of MgO, Al_2O_3, SiO_2, $Mg(OH)_2$, and $Al(OH)_3$ with 6 different compositions (Table 1). The starting compositions were selected to synthesize various kinds of Al-bearing superhydrous phase B, based on our preliminary experiments from which the expected substitution trend of Al-bearing superhydrous phase B was estimated. High-pressure and high-temperature experiments were conducted using a Kawai-type multi-anvil apparatus (ORANGE-2000) at the Geodynamics Research Center, Ehime University, Japan. We used tungsten carbide anvils with a 3-mm truncation. The cell assembly used in this study is shown in Fig. 1. The starting materials were loaded into two gold-palladium double capsules. The experiments were performed at 20 and 24 GPa at 1400 to 2000°C. Heating duration of each run was 1 h.

Temperature was measured using a WRe3%-WRe25% thermocouple, in which the

junction was positioned between the capsules. Temperature gradient across the sample should be ~50°C/mm in these experiments (Inoue, 1994).

The major chemical composition and phases of the recovered samples were determined by SEM-EDS and a micro-focus X-ray diffraction (micro-XRD). The SEM-EDS was operated at 15 kV and 1 nA. Micro-XRD patterns were obtained using CuKα1 radiation (wavelength of 1.5405 Å). The incident X-ray was collimated to 100 μm in diameter.

Water content of the selected samples was quantified using SIMS (SIM-6f, CAMECA) installed at Hokkaido University, Japan. The primary ^{16}O beam operated at 10 kV and 10 nA was focused to a 20-μm diameter location. Secondary ^{1}H and ^{30}Si ions were collected from the central region (10 μm in diameter) of the spattered area. The collected area of the secondary ions was smaller than the typical grain size. The samples for the SIMS were coated with gold to avoid electrostatic charging. Other analytical and instrumental conditions were similar to those used in Yurimoto et al. (1989). Standard materials for quantitative analysis were San Carlos olivine, Mg-endmember superhydrous phase B ($Mg_{10}Si_3H_4O_{18}$) and phase A ($Mg_7Si_2H_6O_{14}$); the H_2O contents of these standard materials were 6-50 ppm, 5.82 wt%, and 11.84 wt%, respectively. Relationship between the H_2O concentration and $^{1}H/^{30}Si$ intensity ratio is shown in Fig. 2.

Results and discussion

Experimental conditions and results are summarized in Table 2. Observed phases include superhydrous phase B, phase B, phase D, δ-AlOOH, periclase, corundum, garnet, and hydrous silicate melt. The hydrous silicate melts existed in all run products (Fig. 3).

Two types of superhydrous phase B coexisted in the run products with composition A at 20 GPa and 1600℃ (Fig. 3a) and with composition F at 24 GPa and 1600 ℃. Based on X-ray diffraction patterns, we identified superhydrous phase B and corundum at the high-temperature part, whereas superhydrous phase B, periclase, and corundum were identified at the low-temperature part at 20 GPa and 1600℃ (Fig. 4). Although both were superhydrous phase B, they were clearly distinguishable in the backscattered electron image (Fig. 3), and their chemical compositions were very different (Fig. 5 and Table 3). For example, chemical compositions of superhydrous phase B coexisting in high and low temperature regions were $Mg_{8.1}Al_{1.9}Si_{2.0}H_{5.9}O_{18}$ and $Mg_{6.7}Al_{3.1}Si_{1.6}H_{7.2}O_{18}$, respectively, in the run products recovered from 20 GPa and 1600℃ with composition A. Moreover, the coexistence of superhydrous phase B with different compositions is expected to have slightly different crystal structures. In this study, we call Mg-rich superhydrous phase B existing in high temperature region “Mg-superhydrous phase B”, and Al-rich superhydrous

130 phase B existing in low temperature region “Al-superhydrous phase B”, based on their
131 compositions.

132 At 24 GPa and 2000℃ with composition A, superhydrous phase B, δ-AlOOH,
133 hydrous silicate melt, and unreacted material was observed (Fig 3b). The chemical
134 composition of superhydrous phase B was $Mg_{7.9}Al_{3.9}Si_{1.3}H_{3.3}O_{18}$. The Al content of
135 superhydrous phase B synthesized at 24 GPa and 2000℃ was higher than that of
136 superhydrous phase B synthesized at 20 GPa and 1600℃. Therefore, this superhydrous
137 phase B is expected to be Al-superhydrous phase B.

138 We succeeded in synthesizing Al-bearing superhydrous phase B with 12 compositions
139 (Fig. 5 and Table 3). The maximum Al_2O_3 content is 31.9(6) wt% with a
140 $Mg_{7.8}Al_{3.9}Si_{1.3}H_{3.4}O_{18}$ chemical formula in the sample synthesized at 24 GPa and 2000℃
141 with composition B. The Al_2O_3 content is substantially higher than those of previous
142 studies (0.2-4.7 wt%; Litasov and Ohtani, 2003; Ghosh and Schmidt, 2014). Figs. 5a-b
143 show the compositional relationships of Al versus Mg and Si, respectively, in superhydrous
144 phase B when the O number is 16 (ignoring H), which is based on this study and previous
145 studies (Litasov and Ohtani, 2003; Ghosh and Schmidt, 2014). The two substitutions were
146 observed in this study. In the case of substitution ① inFig 5, Mg and Si contents of
147 superhydrous phase B gradually decrease with increasing Al content up to Al = ~4 pfu.

addition, there was a tendency for the chemical compositions to be similar between our result and previous studies. In the case of substitution ②, the Mg content increased and the Si content decreased with increasing Al content between Al = 3.5 and 4.0 pfu.

Figs. 5d-f show the compositional relationships of Al versus Mg, Si, and H, respectively, in superhydrous phase B when the O number is 18 (including H). Water content of the closed symbols was measured by SIMS. On the other hand, water content of the open symbols was estimated from relationship between Al and H of Al-bearing superhydrous phase B whose water content can be measured by SIMS in this study (Figs. 5c-f), because it was difficult to obtain the SIMS measurement for these samples due to small grain sizes and inclusions in the crystals. We believe that this estimation is valid because when the Mg and Si contents gradually decrease with increasing Al content (Fig. 5a and b), which indicates that the substitution mechanism in superhydrous phase B does not change up to at least Al = 3 pfu. In Figs 5d-f, which include H_2O content, the two substitutions were clearly observed. In the case of substitution ①, the Mg and the Si contents decreased, and the H content increased with increasing Al content. On the other hand, in the case of substitution ②, the Si and the H contents decreased, and the Mg content increased with Al content. In addition, our result show that the maximum H_2O content is 11.1(3) wt% in Al-bearing superhydrous phase B when Al = 3 pfu (O = 18),

which is ~1.9 times higher than that of its Mg-endmember.

These facts suggest that an Al^{3+}-H^{+} coupled substitution occurs in Al-bearing superhydrous phase B in the substitution ① region. Based on the chemical composition, we propose the following substitution for substitution ①: $2Mg^{2+} + Si^{4+} \rightleftarrows 2Al^{3+} + 2H^{+} + V_{Mg}$ (Mg site vacancy). This substitution can be divided into two substitutions: $2Mg^{2+} \rightleftarrows Al^{3+} + H^{+} + V_{Mg}$ and $Si^{4+} \rightleftarrows Al^{3+} + H^{+}$. When these substitutions occur on al:1 basis, we can explain the change in chemical composition shown in Figs. 5d-f. The Al^{3+}-H^{+} coupled substitution of Si ($Si^{4+} \leftrightarrows Al^{3+}+H^{+}$) was observed in Al-bearing hydrous stishovite (e.g., Smyth et al., 1995; Bromiley et al., 2006). However, in higher Al content of Al-bearing hydrous stishovite, the relationship between Al and H indicated that the water content is much smaller than that expected by Al^{3+}-H^{+} coupled substitution (Al:H = 2.5-7:1) (Litasov et al., 2007). Bromiley et al. (2006) proposed that Al^{3+} substitution for octahedral Si^{4+} can be charge-balanced by coupled substitution of Al^{3+} onto the large, distorted octahedral, interstitial sites in the stishovite structure ($3Si^{4+} \leftrightarrows 3\ Al^{3+}$(octahedral site) + Al^{3+} (interstitial site)). In the case of superhydrous phase B, the relationship between Al and H is 1:1. Therefore, only $Si^{4+} \leftrightarrows Al^{3+} + H^{+}$ substitution occurred in Si site.

In the case of substitution②, we propose the following substitution: $Si^{4+} + 16H^{+} \leftrightarrows 4Mg^{2+} + 4Al^{3+}$. This substitution could be divided into three substitutions: $Mg^{2+} + Si^{4+} \leftrightarrows$

184 $2Al^{3+}$: $Al^{3+} + H^{+} \leftrightarrows 2Mg^{2+}$: $4H^{+} \leftrightarrows Si^{4+}$ = 4 : 4 :3. However, there are some choice to
185 satisfy the substitution ② (e.g., $Si^{4+} \rightleftarrows 4H^{+}$, $Mg^{2+} + Si^{4+} \rightleftarrows 2Al^{2+}$, $3Mg^{2+} \rightleftarrows 2Al^{3+}$). The
186 crystal structure analysis is necessary to clarify the substitution mechanism clearly. In this
187 study, we call substitution ① "hydration substitution", and substitution ② "dehydration
188 substitution", respectively.

189 Fig. 5c shows the relationship between water content and synthesis temperature.
190 Water content increased with increasing synthesis temperature up to 1600°C. On the other
191 hand, water content decreased with increasing synthesis temperature above 1600°C.
192 Therefore, hydration and dehydration substitution occur up to and above 1600°C,
193 respectively.

194 We can predict the compositional boundary between Mg- and Al-superhydrous phase
195 B from a crystallographic standpoint. Al favors the Si octahedral site because of similarities
196 in size. Superhydrous phase B contains Si in both octahedral and tetrahedral sites. 1/3 and
197 2/3 of Si is in octahedral and tetrahedral sites, respectively (Pacalo and Parise, 1992). In
198 addition, $Mg^{2+} = Al^{3+} + H^{+} + V_{Mg}$ and $Si^{4+} = Al^{3+} + H^{+}$ substitution occurred and always
199 keep 1:1 at least up to Al = 4 pfu in the condition below 1600°C. Therefore, we imagine the
200 boundary between the Mg- and Al-superhydrous phase B is Al = 2 pfu. This consideration
201 is consistent with our results. The coexisting superhydrous phase Bs are clearly bounded by

the boundary of Al = 2 (Figs. 5d-f). Above Al = 2 pfu, crystal structure may slightly change because the Si octahedral site is fully occupied by Al. Thus, a single crystal structure refinement is needed.

Fig. 6 shows the Al_2O_3 content in superhydrous phase B as a function of pressure and temperature. Al_2O_3 content increased with increasing temperature up to 2000 °C. Furthermore, we observed the pressure dependence of the Al_2O_3 contents of Mg- and Al-superhydrous phase B. The Al_2O_3 contents of Mg- and Al-superhydrous phase B increased with decreasing pressure. Fig. 6 shows that the synthesis temperature boundary of Mg-SuB and Al-SuB exist at 1600°C.

The stability field of superhydrous phase B(Fig. 7) is expanded from ~1300-1400°C (Ohtani et al., 2003) to at least 2000°C at 20-24 GPa because of Al incorporation. The perfect dehydration or the decomposition of our Al-bearing superhydrous phase B was not observed in our experimental conditions (up to 2000°C at 20-24 GPa). This effect of Al is similar to the case of phase D (Ghosh and Schmidt, 2014; Pamato et al., 2015). In the case of Al-endmember phase D, the Al-Si disorder contributes to the configurational entropy and stabilizes phase D (Pamato et al. 2015). Al is expected to substitute for Si at the octahedral site in superhydrous phase B. Therefore, the Al-Si disorder is expected to occur in Al-bearing superhydrous phase B and to stabilize this phase. In addition, Al-superhydrous

220 phase B started to dehydrate to stabilize at high temperature above 1600°C.

221 The effect of other elements (e.g., Fe, Ca, and Na) on the stability of superhydrous
222 phase B is also important. However, Ca and Na elements should not be contained in
223 superhydrous phase B because the ion radii are much larger than those of Mg and Si.
224 Therefore, we discuss about the effect of Fe on the stability of superhydrous phase B.

225 The effect of Fe on a high temperature stability of phase D was reported by Ghosh
226 and Schmidt (2014) and Pamato et al. (2015). They reported that the destabilizing effect of
227 FeO counteracts the stabilizing effect of Al_2O_3 on phase D. Therefore, Al/Fe ratio is a key
228 factor for the stability of phase D. In the case of superhydrous phase B, the stabilizing
229 effect of Fe_2O_3 was reported by Ganskow and Langenhorst (2014). Therefore,
230 $(Al^{3+}+Fe^{3+})/Fe^{2+}$ ratio is a key factor for the stability of superhydrous phase B. Though the
231 target of this study was to clarify the effect of Al in Mg-endmember superhydrous phase B,
232 further study of the effect of Fe on the stability of superhydrous phase B is necessary to be
233 resolved in near future.

234 Al-bearing phase B was also observed at 24 GPa and 1400°C with composition C.
235 The chemical composition of Al-bearing phase B was MgO 41.4 wt%, Al_2O_3 23.3 wt%,
236 SiO_2 19.3 wt%, and total 84.0 wt%. The chemical formula can be described as
237 $Mg_{8.7}Al_{3.9}Si_{2.7}O_{20}$ when ignoring H_2O (cf. Mg-endmember phaseB: $Mg_{12}Si_4H_2O_{21}$). Mg and

238 Si contents of this phase decreased with increasing Al content, which is the same as
239 superhydrous phase B. Phase B also contains Si in both octahedral and tetrahedral sites
240 (Finger et al., 1989). The same or similar substitution mechanism is expected to occur. Thus,
241 we expect that the stability field of phase B also expands to a higher temperature and the
242 H_2O contents increase by Al substitution, as well as superhydrous phase B. Further study is
243 anticipated for Al-bearing phase B.
244

245 **Implications**

246 In the MgO-SiO_2-H_2O system, water can be transported to the lower mantle by
247 superhydrous phase B and phase D in the cold slab (Fig. 7). On the other hand, Mg-end
248 members of these hydrous phases dehydrate to form bridgmanite + periclase/stishovite +
249 fluid in the stagnant slab, in which the temperatures are lower than that of the normal
250 mantle geotherm. In this case, there are no host hydrous phases of water in the lower mantle
251 along the normal mantle geotherm. However, mantle materials contain some amount of
252 Al_2O_3, thus the Al incorporation in hydrous phases enhance the temperature stability as
253 shown in this study and previous studies (Ghosh and Schmidt, 2014; Pamato et al., 2015).

254 We estimated the amount of Al_2O_3 content in the condition that superhydrous
255 phase B can stably exist at temperatures in the normal mantle geotherm. Fig. 6 shows that

Al-bearing superhydrous phase B, which is synthesized at 1600 °C, has ~15-33 wt% Al_2O_3. Thus, at least 15 wt% of Al_2O_3 is required for superhydrous phase B to stably exist at temperatures of the normal mantle geotherm.

We also calculated the Al partition coefficient between superhydrous phase B and other phases including garnet and bridgmanite (Fig. 8; Litasov and Ohtani, 2003). The element partitioning data of Al between superhydrous phase B and garnet or bridgmanite was determined using $K_D=\left(X_{Mg}^{Gt\ or Brg}\cdot X_{Al}^{SuB}\right)/\left(X_{Al}^{Gt\ or\ Brg}\cdot X_{Mg}^{SuB}\right)$ modified from Frost (2003), here with $X_{Mg\ or\ Al}^{mineral}$ is the molar ratio of mineral of interest. This figure shows that Al becomes easy to distribute to superhydrous phase B with increasing pressure and temperature. Therefore, Al-bearing superhydrous phase B could be stable in subducted slab rocks, which have a high Al_2O_3 content compared to pyrolite (e.g., chlorite) at temperatures of the typical lower-mantle. Thus, water can be transported to the lower mantle even at temperature of the normal mantle geotherm. On the other hand, superhydrous phase B dehydrates in the hydrous pyrolite composition, which is poor in Al_2O_3 (Litasov and Ohtani, 2003).

Acknowledgments

The authors would like to thank T. Shinmei for technical help for the high-pressure

274 experiments, and T. Kawazoe for advice for manuscript writing. S.K. was supported by
275 Research Fellowships of the Japan Society for the Promotion of Science (JSPS) for Young
276 Scientists (DC1). This work was supported by JSPS KAKENHI Grant Numbers 16J0269
277 for S.K. and 26247073, 15H05828 for T.I.. In addition, this work was supported by the
278 Joint Usage/Research Program (2017B24) of PRIUS, Ehime University.

279

References

Bromiley, G.D., Bromiley, F.A., and Bromiley D.W. (2006) On the mechanism for H and AL incorporation in stishovite. Physics and Chemistry of Minerals, 33, 613-621.

Brown, J. M., and Shankland, T.J. (1981) Thermodynamic parameters in the Earth as determined from seismic profiles. Geophysical Journal International, 66, 579–596.

Cai, N., Inoue, T., Fujino, K., Ofuji, H., and Yurimoto, H. A possible new Al-bearing hydrous Mg-silicate (23 Å phase) in the deep upper mantle. American Mineralogist, 100, 2330-2335.

Frost D.J. (2003) The structure and sharpness of $(Mg,Fe)_2SiO_4$ phase transformations in the transition zone. Earth and Planetary Science Letter, 216, 313-328.

Finger, L.W., Ko, J., Hazen, R.M., Gasparik, T, Hemlry, R.J., Prewitt, C.T., and Weidner, D.J. Crsytal chemistry of phase B and an anhydrous analogue: implications for water storage in the upper mantle. Nature, 341, 140-142.

Ganskow, G., and Langenhorst, F. (2014) Stability and crystal chemistry of iron-bearing dense hydrous magnesium silicates. Chemie der Erde, 74, 489-496.

Gasparik, T. (1993) The role of volatiles in the transition zone. Journal of Geophysical Research, 98, 4287-4300.

Ghosh, S., Schmidt, M.W. (2014) Melting of phase D in the lower mantle and implications

for recycling and storage of H_2O in the deep mantle. Geochimica et Cosmochimica Acta, 145, 72-88.

Helffrich, G., and Brodholt, J. (1991) Relationship of deep seismicity to the thermal structure of subducted lithosphere. Nature, 353, 252-255.

Inoue, T. (1994) Effect of water on melting phase relations and melt composition in the system Mg_2SiO_4-$MgSiO_3$-H_2O up to 15 GPa. Physics of the Earth Planetary Interiors, 85, 237-263.

Irifune, T., Kubo, N., Isshiki, M., and Yamasaki, Y. (1998) Phase transformation in serpentine and transportation of water into the lower mantle. Geophysical Research Letter, 25, 203-206.

Katato, S., Paterson, M.S., and FitzGerald, J.D. (1986) Rheology of synthetic olivine aggregates: Influence of grain size and water. Journal of Geophysical Research, 91, 8151-8176.

Kawamoto, T. (2004) Hydrous phase stability and partial melt chemistry in H_2O-saturated KLB-1 peridotite up to the uppermost lower mantle conditions. Physics of the Earth Planetary Interiors, 143-144, 387-395.

Litasov, K., and Ohtani, E. (2003) Stability of various hydrous phases in CMAS-H_2O system up to 25 GPa. Physics and Chemistry of Minerals, 30, 147-156.

316 Litasov, K.D., Kagi, H., Shatskiy, A., Ohtani, E., Lakshtanov, D.L., and Bass, J.B., and Ito,
317 E. (2007) High hydrogen solubility in Al -rich stishovite and water transport in the
318 lower mantle. Earth and Planetary Science Letters, 262, 620-634.
319 Litasov, K.D., Ohtani, E., Nishihara, Y., Suzuki, A., and Funakoshi, K. (2008) Thermal
320 equation of state of Al- and Fe-bearing phase D. Journal of Geophysical Research,
321 113, B08205.
322 Nishi, M., Irifune, T., Tsuchiya, J., Tange, Y., Nishihara, Y., Fujino, K., and Higo, Y. (2014)
323 Stability of hydrous slicate at high pressures and water transport to the deep lower
324 mantle. Nature Geoscience, 7, 224-227.
325 Ohira, I., Ohtani, E., Sakai, T., Miyahara, M., Hirao, N., Ohishi, Y., and Nishijima, M.
326 (2014) Stability of a hydrous δ-phase, AlOOH-$MgSiO_2(OH)_2$, and a mechanism for
327 water transport into the base of lower mantle. Earth and Planetary Science Letter,
328 401, 12-17.
329 Ohtani, E., Touma, M., Litasov, K.D., Kubo, T., and Suzuki, A. (2001) Stability of hydrous
330 phases and water storage capacity in the transitional zone and lower mantle. Physics
331 of the Earth Planetary Interiors, 124, 105-117.
332 Ohtani, E., Toma, M., Kubo, T., Kondo, T., Kikegawa, T. (2003) In situ X-ray observation
333 of decomposition of superhydrous phase B at high pressure and temperature.

Geophysical Research Letter, 30(2), 1029.

Ohtani, E., Litasov, K.D., Hosoya, T., Kubo, T., and Kondo, T. (2004) Water transport into the deep mantle and formation of a hydrous transition zone. Physics of the Earth Planetary Interiors, 143-144, 255-269.

Ono, S. (1998) Stability limits of hydrous minerals in sediment and mid-ocean ridge basalt composition: Implications for water transport in subduction zones. Journal of Geophysical Research, 103, 18253-18257.

Pacalo, R.E.G., and Parise, J.B. (1992) Crystal structure of superhydrous phase B, a hydrous magnesium silicate synthesized at 1400 °C and 20 GPa. American Mineralogist, 77, 681-684.

Pamato, M.G., Myhill, R., Boffa Ballaran, T., Frost, D.J., Heidelbach, F., and Miyajima, N. (2015) Lower-mantle water reservoir implied by the extreme stability of a hydrous aluminosilicate. Nature Geoscience, 8, 75-79.

Pearson, D.G., Brenker, F.E., Nestola, F., McNeill, J., Nasdala, L., Hutchison, M.T., Matveev, S., Mather, K., Silversmit, G., Schmitz, S., Vekemans, B., Vincze, L. (2014) Hydrous mantle transition zone indicated by ringwoodite included within diamond. Science, 507, 221-224.

Schmidt, M.W., Poli, S. (1998) Experimentally based water budgets for dehydrating slabs

and consequences for arc magma generation. Earth and Planetary Science Letter, 163, 361-379.

Smyth, J.R., Swope, R.J, and Pawley, A.J. (1995) H in rutile-type compounds: II. Crystal chemistry of Al substitution in H-bearing stishovite. American Mineralogist, 80, 454-456.

Tsuchiya, T. (2003) First-principles prediction of the P-V-T equation of state of gold and the 660-km discontinuity in Earth's mantle. Earth and Planetary Science Letter, 108, 2462.

Yoshino, T., Matsuzaki, T., Yamashita, S., Katsura, T. (2006) Hydrous olivine unable to account for conductivity anomaly at the top of the asthenosphere. Nature, 443, 973-976.

Yurimoto, H., Kurosawa, M., Sueno, S. (1989) Hydrogen analysis in quartz crystals and quartz glasses by secondary ion mass spectrometry. Geochimica et Cosmochimica Acta, 53, 751-755.

This is a preprint, the final version is subject to change, of the American Mineralogist (MSA)
Cite as Authors (Year) Title. American Mineralogist, in press.
DOI: https://doi.org/10.2138/am-2018-6499

Figure caption

Figure 1. Cell assembly for the high-pressure and temperature experiment.

Figure 2. The calibration line used for the present SIMS measurements of H_2O concentration. Calibration standard materials are San Carlos olivine (SCO), Mg-endmember superhydrous phase B (SuB), and Mg -endmember phase A, which contain 6-50 ppm, 5.82 wt%, and 11.84 wt% H_2O, respectively.

Figure 3. Back scattered electron image of recovered sample from (a) 20 GPa and 1600°C with composition A and(b) 24 GPa and 2000°C with composition A. Circles indicate the positions of X-ray diffraction patterns (Fig. 4). There were two types of superhydrous phase B in the capsule. Al-SuB: Al-superhydrous phase B (Al-rich compared to Mg-SuB), Mg-SuB: Mg-superhydrous phaseB (Al-poor compared to Al-SuB), Pc: periclase, Cor: corundum, Liquid: hydrous silicate melt, δ: δ-AlOOH.

Figure 4. X-ray diffraction patterns of recovered sample from 20 GPa and 1600°C with composition A. The diffraction patterns show both hydrous phases can be indexed as superhydrous phase B, and their crystal structures are similar but slightly different. The

385 diffraction of gold can be seen because of gold coating for the SIMS measurements. SuB
386 and *: superhydrous phase B, Pc: periclase, Cor: corundum, Au: gold, AuPd:
387 gold-palladium.

388

389 **Figure 5.** Al dependence of chemical composition of superhydrous phase B. (a) Mg and (b)
390 Si pfu (per formula unit) when the O = 16 (i.e. H_2O content is ignored.). (c) synthesis
391 temperature dependence of H content. (d) Mg, (e) Si and (f) H when the O = 18. Green
392 circles, red squares, and blue diamonds show Mg, Si, and H, respectively. Green, red, and
393 blue broken lines indicate the Mg, Si, and H tendencies of $2Mg^{2+} + Si^{4+} \rightleftarrows 2Al^{3+} + 2H^{+} +$
394 V_{Mg} substitution, respectively. Green, red, and blue dotted lines indicate the Mg, Si, and H
395 tendencies of $Si^{4+} + 16H^{+} \leftrightarrows 4Al^{3+} + 4H^{+}$ substitution Open symbols indicate that water
396 content of these samples was estimated from the tendency of H in our result (e). Black
397 crosses show composition of Mg-end member superhydrous phase B. Pairs of asterisks and
398 stars represent coexisting Mg- and Al-superhydrous phase Bs. Black dotted lines show
399 boundary between Mg- and Al-superhydrous phase B.

400

401 **Figure 6.** Temperature-pressure dependence of Al_2O_3 content in superhydrous phase B.
402 Blue and red symbols show data at 20-22 and 24-25 GPa, respectively. Error bars are

403 smaller than the symbol sizes. Black dotted line shows boundary between Mg- and
404 Al-superhydrous phase Bs.
405
406 **Figure 7.** Stability of hydrous phases in the MgO-Al_2O_3-SiO_2-H_2O system at the bottom of
407 the transition zone and the uppermost lower mantle. Red diamonds show the conditions
408 where Al-bearing superhydrous phase B is stable (this study). Black solid line indicates
409 stability field of superhydrous phase B in the MgO-SiO_2-H_2O system. Blue and orange
410 solid lines show the decomposition boundary of phase D in the MgO-Al_2O_3-SiO_2-H_2O with
411 1 wt% Al_2O_3 content and the Al_2O_3-SiO_2-H_2O system, respectively (Ghosh and Schmidt,
412 2013; Pamato et al., 2015). Dotted line is post-spinel transformation boundary (Tsuchiya,
413 2003). Geotherms of the normal mantle (Brown and Shankland, 1981) and cold slab
414 (Helffrich and Brodholt, 1991) are schematically shown in this figure. The temperature path
415 of the stagnant slab is schematically given in this figure. Al-bearing superhydrous phase B
416 can be stable in a subducted slab with high Al content at temperatures of the typical lower
417 mantle. Brg: bridgmanite, Pc: periclase, Rw: ringwoodite, hRw: hydrous ringwoodite, St:
418 stishovite, B: phase B, SuB; superhydrous phase B, D: phase D, Al-D: Al-end member
419 phase D, L: liquid.
420

421 **Figure 8.** Partition coefficient of Al between (a) superhydrous phase B and garnet, (b)
422 superhydrous phase B and bridgmanite. Original data comes from Litasov and Ohtani
423 (2003). The bulk composition describes as below: 45.15 wt% SiO_2, 5.20 wt% Al_2O_3, 43.46
424 wt% MgO, 4.19 wt% CaO and 2.00 wt % H_2O. Error bars are smaller than the symbol sizes.
425 SuB: superhydrous phase B, Gt: garnet, Brg: bridgmanite.
426

This is a preprint, the final version is subject to change, of the American Mineralogist (MSA)
Cite as Authors (Year) Title. American Mineralogist, in press.
DOI: https://doi.org/10.2138/am-2018-6499

Table 1 Compositions of starting materials used in the study

(wt%)	A	B	C	D	E	F
MgO	50.1	44.5	57.9	53.1	58.9	65.0
Al_2O_3	25.8	23.2	8.1	16.8	14.7	6.9
SiO_2	13.6	14.2	24.0	19.8	16.0	17.7
H_2O	10.4	18.1	10.1	8.0	10.4	10.4
total	100	100	100	100	100	100

427

This is a preprint, the final version is subject to change, of the American Mineralogist (MSA)
Cite as Authors (Year) Title. American Mineralogist, in press.
DOI: https://doi.org/10.2138/am-2018-6499

Table 2. Experimental conditions and results

Run No.	Pressure (GPa)	Temperature (°C)	Starting materials	Phase
OS2933	20	1600	A	Al-SuB, Mg-SuB, Cor, Pc, melt
			B	Al-SuB, δ, melt
OS2824	24	1600	A	Al-SuB, δ, melt, (Pc, Cor, Gt)
OS2804	24	1800	A	Al-SuB, δ, melt, (Pc, Cor, Gt)
			B	Al-SuB, δ, melt
OS2827	24	2000	A	Al-SuB, δ, melt, (Pc, Cor, Gt)
			B	Al-SuB, δ, melt, (Pc, Gt)
OS2941	24	1400	C	Mg-SuB, B, Pc, melt
			D	Mg-SuB, D, Pc, melt
OS2886	24	1600	E	Pc, Gt, melt
			F	Al-SuB, Mg-SuB, δ, Pc, Cor, melt

Note: (a) The inside of parenthesis is unreacted materials on low temperature side. (b) Abbreviations are as follows: Al-SuB: Al-superhydrous phase B, Mg-SuB: Mg-superhydrous phase B, δ: δ-AlOOH, B: phase B, D: phase D, Pc: periclase, Cor: corundum, Gt: garnet, melt: hydrous silicate melt.

428

This is a preprint, the final version is subject to change, of the American Mineralogist (MSA)
Cite as Authors (Year) Title. American Mineralogist, in press.
DOI: https://doi.org/10.2138/am-2018-6499

Table 3. Chemical composition of superhydrous phase B

Starting material		A					B			C	D	F	
Sample	Mg-end SuB	Mg-SuB	Al-SuB	Al-SuB	Al-SuB	Al-SuB	Al-SuB	Al-SuB	Al-SuB	Mg-SuB	Mg-SuB	Mg-SuB	Al-SuB
Pressure (GPa)	-	20	20	24	24	24	20	24	24	24	24	24	24
Temperature (°C)	-	1600	1600	1600	1800	2000	1600	1800	2000	1400	1400	1600	1600
MgO	65.1	54.6(16)	46.0(12)	48.6(5)	50.1(6)	51.0(6)	43.6(7)	49.8(8)	50.6(12)	60.3(9)	57.5(6)	56.4(10)	50.8(16)
Al_2O_3	0	16.2(6)	26.6(2)	27.9(8)	30.2(10)	31.9(8)	29.3(9)	31.7(2)	31.9(6)	7.1(3)	10.8(2)	14.0(7)	22.9(8)
SiO_2	29.1	20.3(6)	16.3(2)	15.3(2)	13.5(1)	12.4(1)	16.1(2)	12.5(3)	12.7(5)	26.0(2)	24.0(3)	21.2(3)	17.5(6)
H_2O	5.82	8.9*	11.1(3)	8.2(5)	6.2(4)	4.7(3)	11.0(3)	6.0(4)	4.9(3)	6.6(2)	7.7*	8.4*	8.8(3)
total (wt%)	100	100	100	100	100	100	100	100	100	100	100	100	100
Mg	10	8.13	6.66	7.25	7.65	7.91	6.31	7.63	7.83	9.16	8.65	8.44	7.54
Al	0	1.91	3.05	3.29	3.64	3.91	3.35	3.83	3.9	0.85	1.28	1.66	2.69
Si	3	2.02	1.58	1.53	1.38	1.29	1.56	1.28	1.32	2.65	2.42	2.12	1.75
H	4	5.92	7.20	5.50	4.24	3.28	7.08	4.11	3.36	4.51	5.17	5.86	5.86
cation sum	17	17.98	18.49	17.57	16.92	16.39	18.30	16.86	16.41	17.17	17.52	18.08	17.84
O	18	18	18	18	18	18	18	18	18	18	18	18	18

Note: (a) Total weight was normalized to 100 wt%. (b) *H_2O content was estimated from the tendency of H in our result.

This is a preprint, the final version is subject to change, of the American Mineralogist (MSA)
Cite as Authors (Year) Title. American Mineralogist, in press.
DOI: https://doi.org/10.2138/am-2018-6499

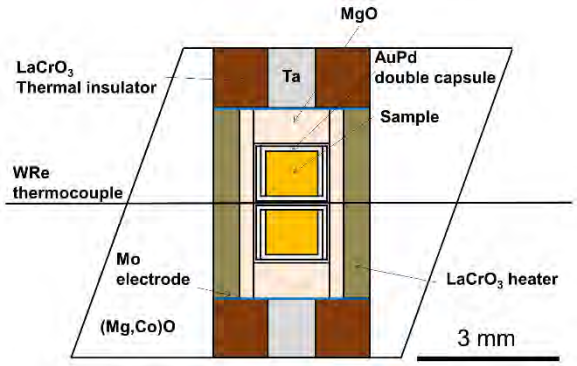

Figure 1

This is a preprint, the final version is subject to change, of the American Mineralogist (MSA)
Cite as Authors (Year) Title. American Mineralogist, in press.
DOI: https://doi.org/10.2138/am-2018-6499

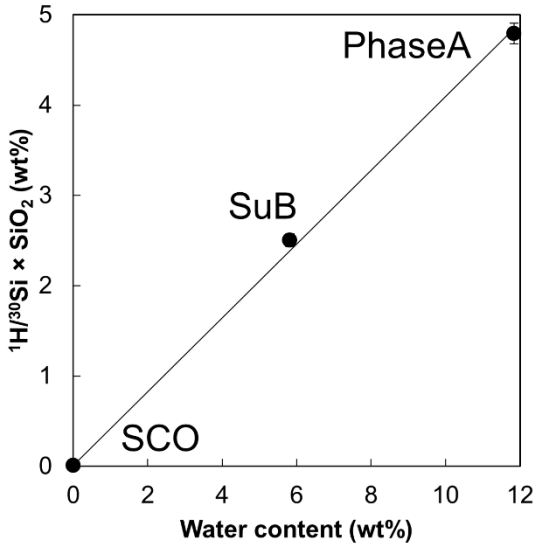

431 Figure 2

This is a preprint, the final version is subject to change, of the American Mineralogist (MSA)
Cite as Authors (Year) Title. American Mineralogist, in press.
DOI: https://doi.org/10.2138/am-2018-6499

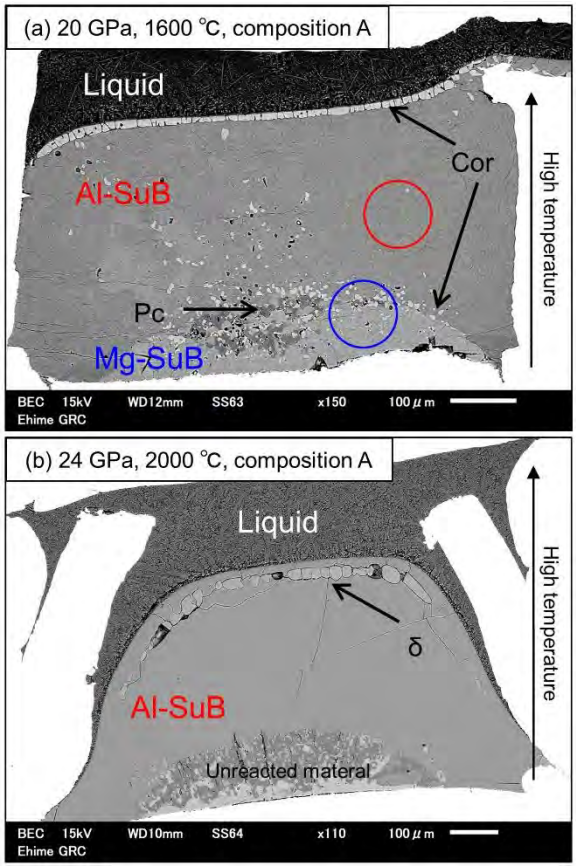

Figure 3

This is a preprint, the final version is subject to change, of the American Mineralogist (MSA)
Cite as Authors (Year) Title. American Mineralogist, in press.
DOI: https://doi.org/10.2138/am-2018-6499

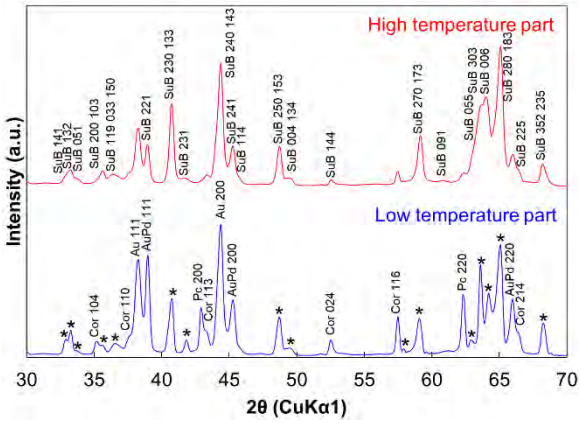

Figure 4

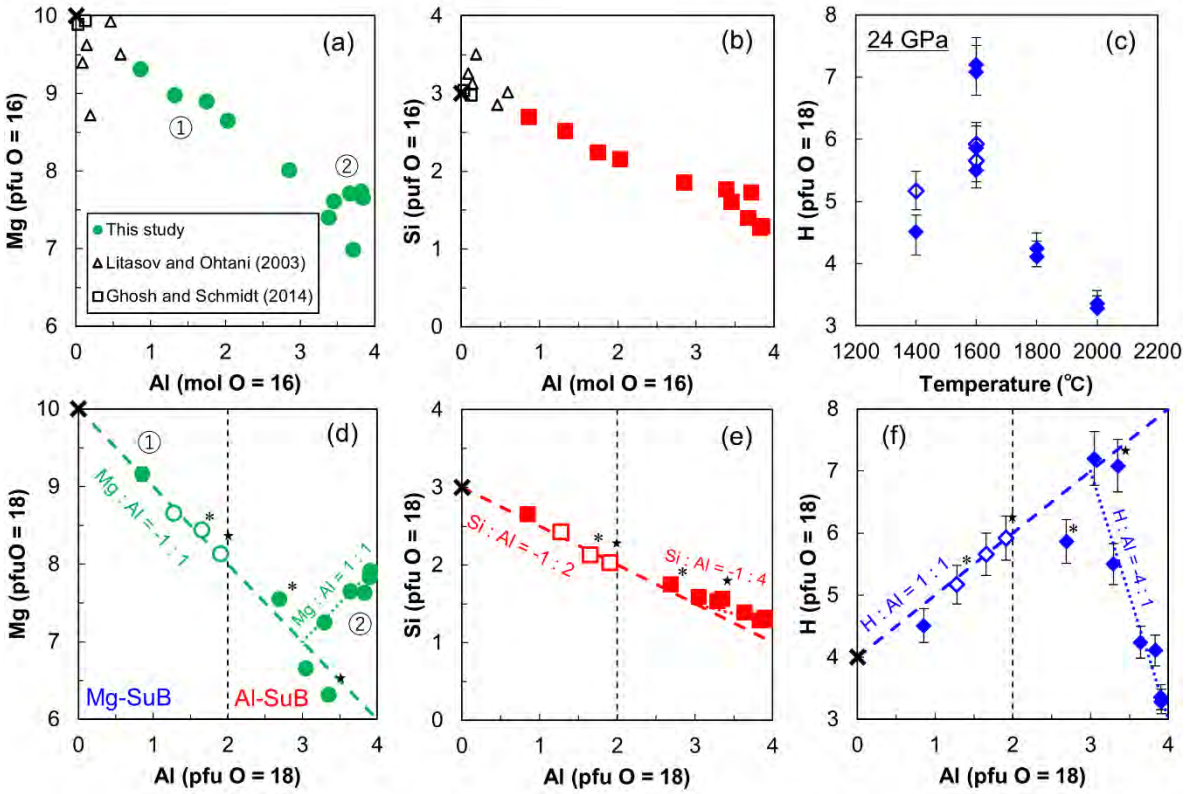

Figure 5

This is a preprint, the final version is subject to change, of the American Mineralogist (MSA)
Cite as Authors (Year) Title. American Mineralogist, in press.
DOI: https://doi.org/10.2138/am-2018-6499

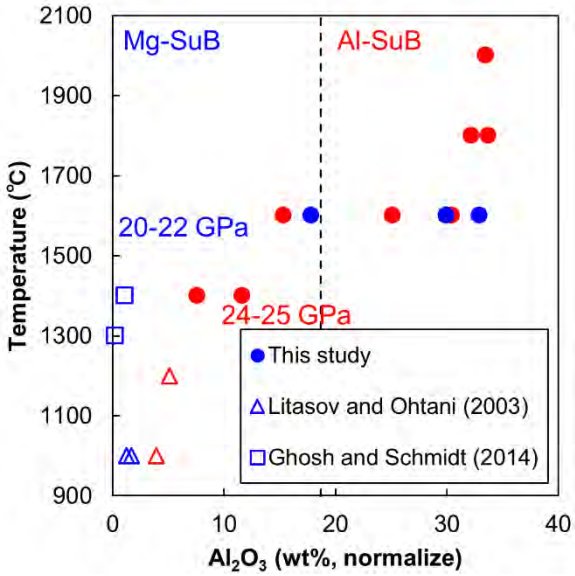

Figure 6

This is a preprint, the final version is subject to change, of the American Mineralogist (MSA)
Cite as Authors (Year) Title. American Mineralogist, in press.
DOI: https://doi.org/10.2138/am-2018-6499

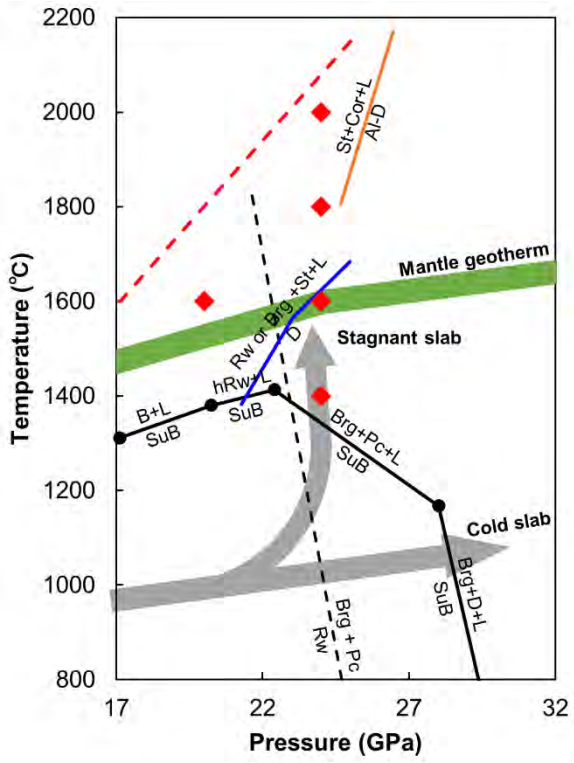

441

442 Figure 7

This is a preprint, the final version is subject to change, of the American Mineralogist (MSA)
Cite as Authors (Year) Title. American Mineralogist, in press.
DOI: https://doi.org/10.2138/am-2018-6499

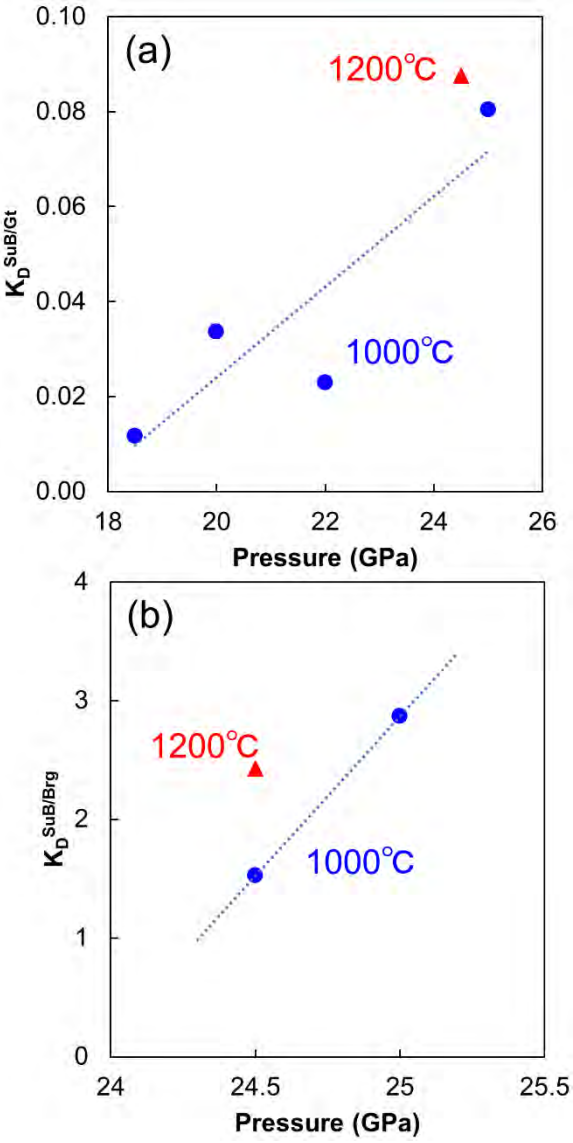

443

444 Figure 8